Current Research in Food Science 10 (2025) 101021

Contents lists available at ScienceDirect

Current Research in Food Science

journal homepage: www.sciencedirect.com/journal/current-research-in-food-science

Encapsulation of menthol by cyclodextrins-comparison between experiments and molecular simulations

Sa Xu [a], Fang Wei [a], Ximing Xu [c], Rui Wang [b], Xiujuan Xu [b], Wu Fan [a,b], Guobi Chai [a,b], Qidong Zhang [a,b], Qingzhao Shi [a,b,*]

[a] College of Chemistry, Zhengzhou University, No 100 of Kexue Road, Zhengzhou, 450001, PR China
[b] Key Laboratory of Tobacco Flavor Basic Research of China National Tobacco Corporation, Zhengzhou Tobacco Research Institute of China National Tobacco Corporation, Zhengzhou, 450000, PR China
[c] Marine Biomedical Institute of Qingdao, School of Medicine and Pharmacy, Ocean University of China, Qingdao, 266580, PR China

ARTICLE INFO

Keywords:
Cyclodextrins
Menthol
Encapsulation
Molecular simulation
Bind free energy

ABSTRACT

Cyclodextrins (CDs) are a traditional wall material for encapsulating flavor ingredients. Given the substantial structural differences among flavor ingredients, experimentally deriving the selection criteria for CDs suitable for these flavor substances is a time-consuming process. However, most existing literature relies on the embedding efficiency from practical experiments to evaluate the binding effect between flavor ingredients and CDs. This article used menthol as the research subject and investigated the binding effects of three different CDs through experiments and computer simulations. The experimental results revealed that β-CD exhibited the optimal encapsulation efficiency (EE, 36.54%) on menthol, subsequently, γ-CD showed a 33.35% EE value, whereas α-CD was unable to form an inclusion complex (IC) with menthol. Conformation changes, root mean square deviation (RMSD), radius of gyration (Rg), Radial distribution function (RDF), solvent accessible surface area (SASA), and hydrogen bonds, and binding free energy were analyzed through molecular dynamics simulation and compared with the experimental results. The results indicated that the IC formed between β-CD and menthol (menthol/β-CD-IC) is the most stable, with a binding free energy (ΔGbind) of −7.27 kcal/mol. The IC formed between α-CD and menthol (menthol/α-CD-IC) is the least stable one (ΔGbind = 2.59 kcal/mol). The results revealed a high degree of consistency between the experimental outcomes and those of molecular simulation, so molecular simulation can serve as a more efficient screening method, an alternative to practical experiments, to obtain the combination ability between host-guest molecules.

1. Introduction

CDs are extensively applied in flavors, pharmaceuticals, and food industries. They can extend the release time of aroma in flavors, prolong the shelf-life of medicines, and stabilize food flavors. Besides being cost-effective, CD-based encapsulation products are easy to prepare. Most importantly, CDs have obtained safety recognition from the food industry, and they are among the few edible encapsulating wall materials (Han et al., 2021; Hu et al., 2021; Phunpee et al., 2016; Xiao et al., 2019). Common natural CDs are α-CD, β-CD, and γ-CD, including 6, 7, and 8 α-1,4-glycosidic bonds in their molecule, respectively (Yin et al., 2021). They all have a hydrophobic cavity and a hydrophilic outer surface and can encapsulate different kinds of guest molecules (Alvira, 2018; Cao et al., 2022; Lin et al., 2022). However, given the substantial structural differences both among flavor ingredients and pharmaceutical molecules, experimentally deriving the selection criteria for CDs suitable for these guest molecules is a time-consuming process. However, most existing literature relies on the embedding efficiency from practical experiments to evaluate the binding effect between guest molecules and CDs (He et al., 2023; Zhang et al., 2022).

As an emerging research method, MD simulation has been widely used to study the binding mechanisms of proteins and small molecules (Hu et al., 2023). Specific to CDs and flavor ingredients inclusion complexes (ICs), MD simulation has been used to explore the conformations and thermodynamic energy changes of CDs binding with small molecules (Bhardwaj and Purohit, 2023; Kumar and Purohit, 2024; Mazurek et al., 2021). For example, Deng et al. investigated the formation and stability mechanisms of β-CD complexes with five C10 aromatic

* Corresponding author. College of Chemistry, Zhengzhou University, No 100 of Kexue Road, Zhengzhou, 450001, PR China.
E-mail address: qingzhao0813@163.com (Q. Shi).

https://doi.org/10.1016/j.crfs.2025.101021
Received 14 January 2025; Received in revised form 24 February 2025; Accepted 3 March 2025
Available online 3 March 2025

molecules through MD simulation, the results indicated that the main driving force for the entry of aroma molecules into the cavity of β-CD is van der Waals interactions (Deng et al., 2022). Pramod Kumar et al. demonstrated that CDs and their derivatives can be used to encapsulate poorly water-soluble compounds through molecular simulations, and the binding free energy of CUR with β-CD, hydroxypropyl-β-CD (HP-β-CD), and 2,6-Di-O-methyl-β-CD (DM-β-CD) was calculated using molecular simulation methods (Kumar et al., 2024). MD simulation may be a more efficient screening method, an alternative to practical experiments, to obtain the binding ability between host-guest molecules. However, to our knowledge, few studies evaluated the consistency of results between practical experiments and computer simulations.

Menthol (Fig. 1A) is a naturally occurring volatile cyclic terpene alcohol with a characteristic minty aroma, commonly found in plants of the mint genus (Hu et al., 2021; Kamatou et al., 2013). Menthol's applications were limited in food, pharmaceuticals, and cosmetics due to the low water solubility and high volatility (Galeotti N, 2002; Silva, 2020; Yildiz et al., 2018), therefore encapsulation treatment is always needed. Previous studies have shown that the solubility and thermodynamic stability of menthol is significantly improved after being encapsulated in CD; however, the mechanism of interaction between menthol and cyclodextrin has not been investigated (Hu et al., 2021; Yildiz et al., 2018).

In this study, menthol was selected as the research subject. The encapsulation effects of different CDs on menthol were analyzed from both experimental and simulation perspectives. Subsequently, a comparison was made between the experimental results and the simulation results. The ICs were characterized using Fourier transform infrared spectroscopy (FTIR), X-ray diffraction (XRD), and Thermogravimetric analysis (TGA) methods. The encapsulation ability was obtained using GC-MS. Molecular dynamics simulations were employed to obtain the conformational and molecular structural changes, RMSD, Rg, RDF, SASA and hydrogen bonds explaining the interaction patterns between menthol and CDs at the microscopic level, and the thermodynamic properties of the ICs were also analyzed.

2. Materials and methods

2.1. Materials

Menthol (>97%) was acquired from Coolaber (Beijing, China), α-CD (98%), and β- CD (99%) were acquired from Innochem (Beijing, China), and γ-CD (99%) was purchased from MACKLIN (Shanghai, China). Ethanol (GR) was purchased from Merck (Jiangsu, China).

2.2. Preparation of inclusion complexes of menthol and CD (menthol/CD-ICs) and physical mixtures

The preparation of menthol/CD-ICs was carried out as previously described (Lin et al., 2022). The CDs (1 mmol) were dissolved in 30 mL distilled water, and 156.3 mg (1 mmol) menthol was dissolved in 5.5 mL ethanol. Then, the menthol solution was slowly added to the CDs solution, stirred at 50 °C for 3 h, cooled to room temperature, and stored in a 4 °C refrigerator. After 24 h, the solution was filtered, and the residue was washed thrice with about 5 mL ethanol. The obtained samples were then dried in a 40 °C drying oven for 3 h. The final IC samples were stored in a desiccator at 4 °C for future use. Menthol and CD with equal molar ratios were weighed and mixed to obtain the menthol/CD physical mixtures.

2.3. Characterization of menthol/CD-ICs

2.3.1. FTIR analysis

The menthol, CDs, menthol/CD-ICs, and menthol/CD physical mixes were measured using an FTIR spectrometer (RX-3050TX + IR Tracer-100+GCMS-TQ8050 NX, Japan), solid samples were ground after mixing with dried KBr. In contrast, liquid samples were dripped onto the middle of KBr pellets. Before the sample measurement, a KBr sample was measured for background subtraction to reduce the effects of H_2O and CO_2 in the air on the sample. The scanning range was 4000-400 cm^{-1}, with each sample scanned 64 times at a resolution of 4 cm^{-1}.

2.3.2. XRD analysis

XRD analysis on menthol, CDs, menthol/CD-ICs, and the physical mixtures was conducted using a CT scanning X-ray diffractometer system (Empyrean, the Netherlands) within the 2θ = 5–50 °C range.

2.3.3. TGA analysis

A thermal analysis system (TA449F3, Germany NETZSCH) was used to conduct thermogravimetric analysis on menthol, CDs, and menthol/CD-ICs. Among them, menthol was ground before the TGA measurement, while the other samples were in powder form and could be

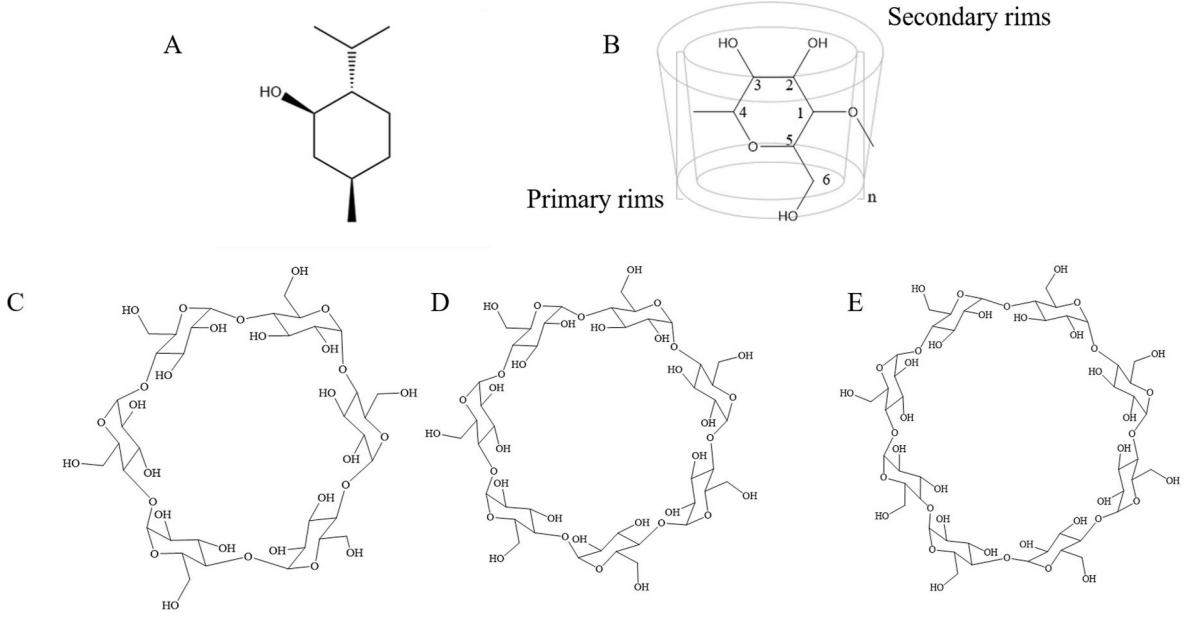

Fig. 1. (A) Chemical structure of menthol. (B) Structure of cyclodextrin glucose units. (C), (D), (E) are the 2D structures of α-CD, β-CD, and γ-CD, respectively.

directly used for TGA testing. Specifically, about 10 mg sample was heated from 30 °C to 600 °C at a rate of 10 °C/min in the Ar atmosphere.

2.4. Determination of EE and loading efficiency (LE)

Menthol (25 mg) was added into a 25 mL volumetric flask and diluted with anhydrous ethanol and prepared standard solutions with concentration gradients of 20 μg/mL, 30 μg/mL, 40 μg/mL, 50 μg/mL, 60 μg/mL, and 70 μg/mL. The peak area was measured using GC-MS (7890 A GC, 5975C MSD, Agilent Technologies, Inc., Santa Clara, CA, USA), separation processes were performed using a DB-5 (60 m × 0.25 mm i. d. × 0.25 μm d. f.), the split ratio was 20:1, and the injection volume was 1 μL. The temperature program increases at 5 °C/min from 50 °C to 200 °C. Plot the standard curve with menthol concentration on the x-axis and peak area on the y-axis (Hu et al., 2021; Shi et al., 2023).

Menthol/CD-ICs (25 mg) were added into a 25 mL volumetric flask and diluted with anhydrous ethanol. Ultrasonicate for 40 min to allow menthol to transfer from the CD cavity into the ethanol phase (Han et al., 2021; Yin et al., 2021). Filter using a microporous membrane and measure the corresponding peak area. The LE and EE of menthol were calculated using the following formulas:

$$EE\ (\%) = (M_E / M_T) \times 100 \quad (1)$$

$$LE\ (\%) = (M_E / M_I) \times 100 \quad (2)$$

Here, M_E refers to the mass of encapsulated menthol, M_T is the mass of menthol initially added, and M_I is the mass of the ICs.

2.5. Computational study

2.5.1. Molecular docking

The host-guest interactions between menthol and CDs were investigated through AutoDock Vina1.1.2 (Eberhardt et al., 2021; Trott and Olson, 2009). The structure of CDs was obtained from the CCDC crystal database, while the structures of menthol were obtained from the PubChem database (PubChem ID 16666) (Kim et al., 2018). AutodockTools (ADT, version 1.5.6) was used to add hydrogen atoms and charges to menthol and CDs, and all rotatable bonds in menthol were released, the distance between the two grids was 0.375 A, and the box size was set to 40 × 40 × 40 A. Each docking process was conducted independently 20 times. Conformations were selected based on binding energy as the starting conformation for the MD simulation.

2.5.2. Molecular dynamics (MD) simulation

MD simulations were used according to previous methods with some modifications (Deng et al., 2022; Kou et al., 2023). The conformations obtained from molecular docking were used as the initial structure for the simulations. MD simulations were conducted using the GROMACS 2023.2 software package with the CHARMM36-jul2022 force field. The force field parameters for menthol and CDs were generated using the CGenFF server (Vanommeslaeghe et al., 2009), and these parameters were converted to GROMACS format using the Python script cgenff_charmm2gmx_py2.py. All simulations utilized periodic boundary conditions, placing molecules in a cubic box with a side length of 4 nm. Energy minimization was performed using the steepest descent method for 50,000 steps, followed by 100 ps of pre-equilibration using NVT and NPT ensembles. In the NVT ensemble, a modified Berendsen thermostat (V-rescale) was used to raise the temperature to 298.15 K. In contrast, in the NPT ensemble, the Parrinello-Rahman barostat controlled the pressure at 1 bar. To elucidate the reason why menthol and α-CD failed to form an IC, we conducted a 200 ns MD simulation on the menthol/α-CD-ICs. In contrast, the menthol/β-CD-ICs and menthol/γ-CD-ICs were simulated for 100 ns. Conformation changes, RMSD (including hydrogen atoms), Rg, RDF, SASA, and hydrogen bonds were analyzed using the commands included in the GROMACS 2023.2 software package. In the thermodynamic analysis, binding free energy calculations for the ICs were conducted using the Molecular Mechanics Poisson-Boltzmann surface area (MM/PBSA) method implemented in the gmx_MMPBSA 1.6.1 program (Valdés-Tresanco et al., 2021), and interaction entropy (Duan et al., 2016) was also calculated. Visualization of the data was carried out by VMD software.

3. Results and discussion

3.1. EE and LE analysis

The quantification of menthol was performed using the GC-MS method, resulting in a linear curve for menthol expressed as y = 1787.89x-14108.31 (R^2 = 0.9988). The EE and LE values of menthol in three CDs were listed in Table 1. When preparing the menthol/α-CD IC, no sediment was observed, implying that menthol and α-CD did not form an effective combination. This finding is consistent with the results previously published by other researchers (He et al., 2023). Among the three CDs, β-CD demonstrated the best encapsulation performance for menthol, with the EE and LE values of β-CD for menthol were 36.54% and 5.81%, respectively, while those of γ-CD for menthol were 33.35% and 4.78%, respectively. The EE and LE values provide references for dosage, cost, and effectiveness for the use of encapsulated products in the food industry. In the pubilshed study (Hu et al., 2021), the EE of menthol/β-CD and menthol/γ-CD were below 20%. The discrepancies between our data and the reported data may be attributed to the different preparation methods.

3.2. Characterization analysis

3.2.1. FTIR analysis

The infrared spectra of menthol, β-CD, γ-CD, the ICs and the menthol/CD physical mixtures are shown in Fig. 2. The OH stretching vibration of menthol was observed at 3262 cm^{-1}, the C-H stretching vibration was observed in the range of 2848–2957 cm^{-1}, and the C-O stretching vibration appeared at 1044 and 1027 cm^{-1} (Phunpee et al., 2016). In the infrared spectra of β-CD and γ-CD, the characteristic absorption peak for the α-glycosidic bond was at 855 cm^{-1}, with C-C bending vibrations at 1080 cm^{-1} and C-O stretching vibrations at 1025/1028 cm^{-1}. The O-H stretching vibration peaks were found at 3340 cm^{-1} and 3370 cm^{-1}, while the C-H stretching and bending vibration peaks were at 2925/2930 cm^{-1} and 1641/1644 cm^{-1}, respectively. In the spectra of the physical mixtures, menthol's characteristic peak was observed at 2848-2957 cm^{-1}. Compared with that of menthol, the characteristic peak in the spectra of menthol/CD-ICs at 2848-2957 cm^{-1} disappeared, indicating that menthol was successfully encapsulated within the cavity of the CDs, which was consistent with previously published results (Chang et al., 2023; Xiao et al., 2019; Yin et al., 2021).

3.2.2. XRD analysis

The XRD patterns of menthol, β-CD, γ-CD, the ICs, and physical mixtures are shown in Fig. 3. Menthol exhibited robust and sharp diffraction peaks at 2θ = 8.2, 12.5, 14.1, 16.3, 17.1, 20.3, and 21.7, demonstrating typical crystalline properties. The XRD pattern of the physical mixtures showed an overlay of the spectra of menthol and CDs. Some new diffraction peaks appeared in the XRD pattern of the ICs. For example, for menthol/β-CD-IC, new diffraction peaks were observed at

Table 1
EE and LE of menthol in CDs.

	menthol/α-CD-IC	menthol/β-CD-IC[a]	menthol/γ-CD-IC[a]
EE	/	36.54 ± 2%	33.35 ± 1.5%
LE	/	5.81 ± 0.7%	4.78 ± 0.2%

Note: [a] Average value ± standard deviation, "/" presents that the IC does not exist.

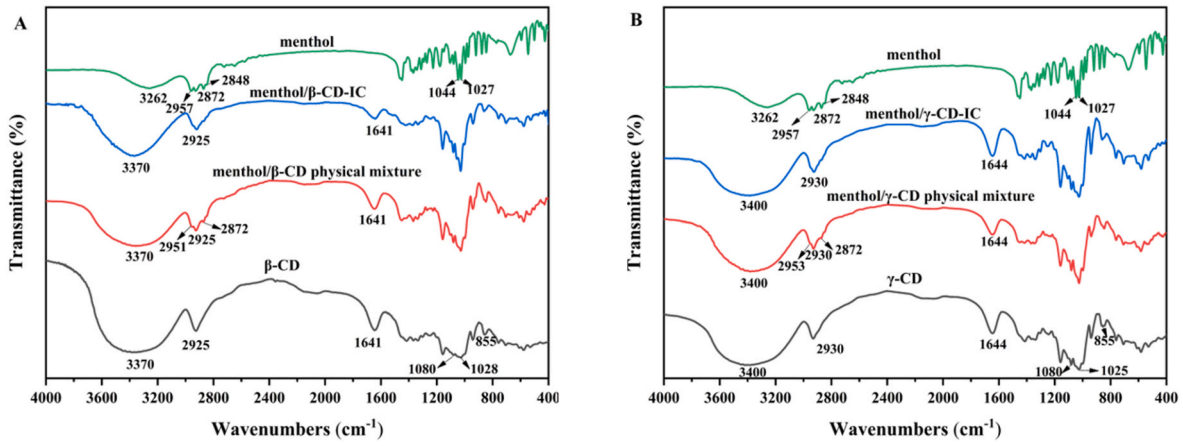

Fig. 2. FTIR spectra of menthol, CDs, menthol/CD-ICs, and physical mixtures. A for β-CD, B for γ-CD.

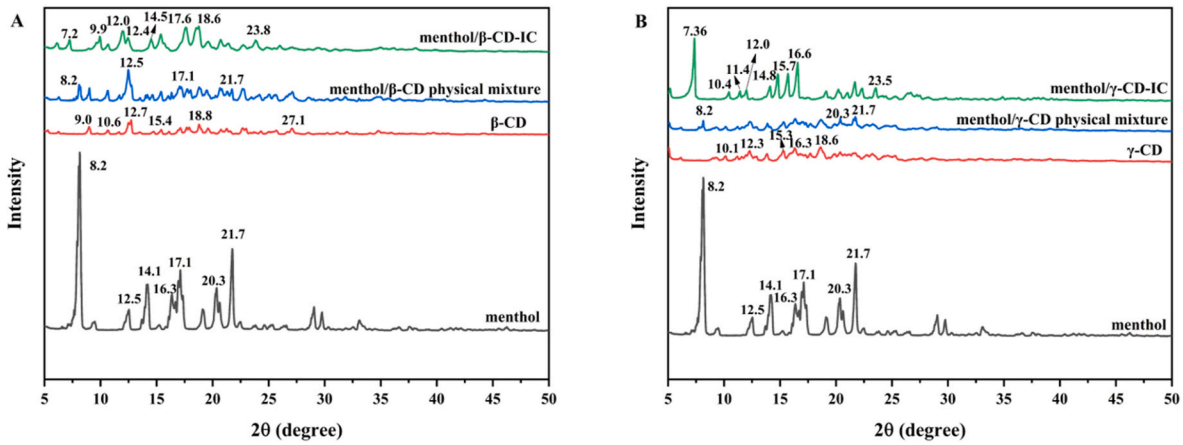

Fig. 3. XRD patterns of menthol, CDs, menthol/CD-ICs, and physical mixtures. A for β-CD, B for γ-CD.

2θ = 7.2, 9.9, 12.0, 12.4, 14.5, 17.6, 18.6, and 23.8. For menthol/γ-CD-IC, new diffraction peaks were observed at 2θ = 7.36, 10.4, 11.4, 12.0, 14.8, 15.7, 16.6, and 23.5. Compared with free CDs, menthol/CD-ICs exhibit an enhanced crystalline property, suggesting that menthol has been successfully incorporated into the internal cavity of the CDs, leading to the formation of a more ordered and structured IC. (Kou et al., 2023; Wu et al., 2020).

3.2.3. TGA analysis

As shown in Fig. 4, menthol completely evaporated at 180 °C. The β-CD, γ-CD, and menthol/β-CD-IC, menthol/γ-CD-IC experienced a weight loss stage at 120 °C, corresponding to the evaporation of water molecules. The second stage of weight loss for β-CD, γ-CD occurred in the range of 290–340 °C, while the second weight loss stage for the menthol/β-CD-IC and menthol/γ-CD-IC occurred in the range of 275–340 °C. In the curve of the two menthol/CD-ICs, no weight loss was observed at 180 °C, indicating that the stability of menthol had been significantly enhanced following its encapsulation within β-CD and γ-CD (Hu et al., 2021).

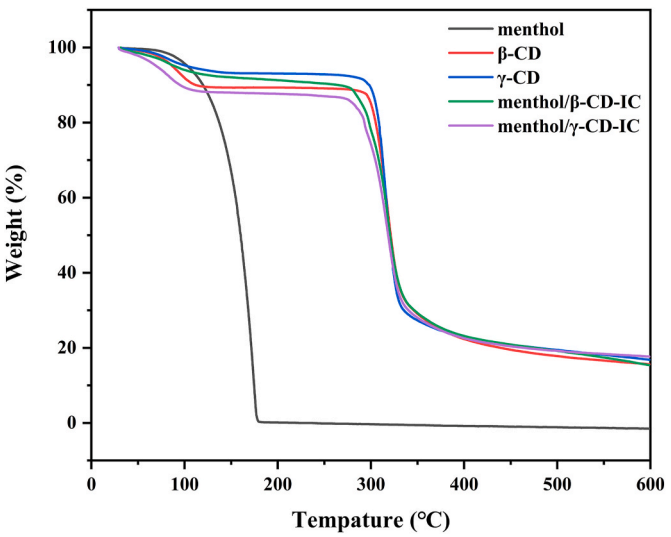

Fig. 4. Thermogravimetric analysis of menthol, β-CD, γ-CD, and menthol/β-CD, γ-CD-ICs.

3.3. Molecular docking and molecular simulation

3.3.1. Molecular docking analysis

Molecular docking was carried out to identify and acquire the conformation characterized by the lowest energy state. As shown in Fig. 5, the molecular docking results revealed that menthol assumes two distinct orientations within the CDs. Specifically, the isopropyl group of menthol takes on configuration I when positioned at the wide edge of the CDs, while it adopts configuration II when located at the narrow edge. Since the binding energy obtained from molecular docking values of the two configurations are quite close (Table 2), both orientations were used

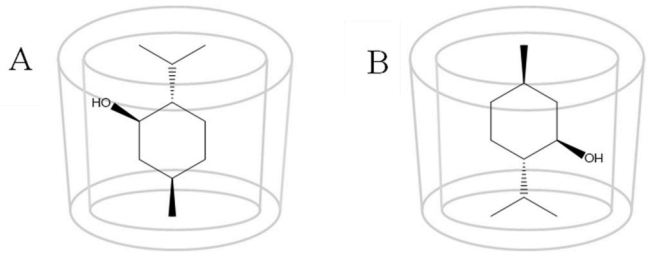

Fig. 5. Two conformations of menthol and CD combination(A) menthol/CD-I (B) menthol/CD-II.

Table 2
The binding energy of the two conformations of menthol and CDs obtained from molecular docking.

IC	binding energy (kcal/mol)
menthol/α-CD-I	−3.5
menthol/α-CD-II	−3.4
menthol/β-CD-I	−4.0
menthol/β-CD-II	−4.1
menthol/γ-CD-I	−3.6
menthol/γ-CD-II	−3.6

for the MD simulation analysis.

3.3.2. *Conformational analysis*

As shown in Fig. 6, snapshots of the conformations of menthol/α-CD-ICs were taken at 0, 40, 80, 120, 160, and 200 ns, while that of menthol/β-CD-ICs and menthol/γ-CD-ICs were taken at 0, 20, 40, 60, 80, and 100 ns. The cavity volume and shape of CDs and menthol are generally consistent with those published in other studies (Kumar et al., 2023; Wang and Meng, 2017). In the case of menthol/α-CD-I, at 0 ns, the methyl group and part of the six-membered ring of menthol entered the cavity of α-CD. By 40 ns, the menthol molecule was located outside the cavity of α-CD and maintained this position without entering the cavity until the end of the simulation. For menthol/α-CD-II, at 0 ns, only the isopropyl group was in the cavity of α-CD, while other parts of the molecule were outside. At 40 ns, the menthol molecule moved outside the cavity. At 80 ns and 120 ns, it was observed that menthol moved further away from the α-CD molecule. By 160 ns, the methyl group and part of the six-membered ring re-entered the cavity and moved outside again by 200 ns. This result suggested that the combination of α-CD with both orientations of the menthol molecule is unstable during the simulation process, which supports the experimental result that menthol/α-CD-IC cannot be formed. This may be due to the smaller cavity volume of α-CD (174 A^3) (Crini, 2014; J, 1998) compared with the molecular volume of menthol (291.5 A^3, calculated through the molar volume of menthol obtained from the ChemSpider database and divided by NA).

Conformational snapshots of menthol/β-CD-I showed that the methyl group and six-membered ring of the menthol molecule consistently remained within the cavity of β-CD. By 80 ns, the isopropyl group of menthol had migrated outside, most probably as a result of steric hindrance. For menthol/β-CD-II, the isopropyl group maintained its position within the cavity, while part of the six-membered ring and

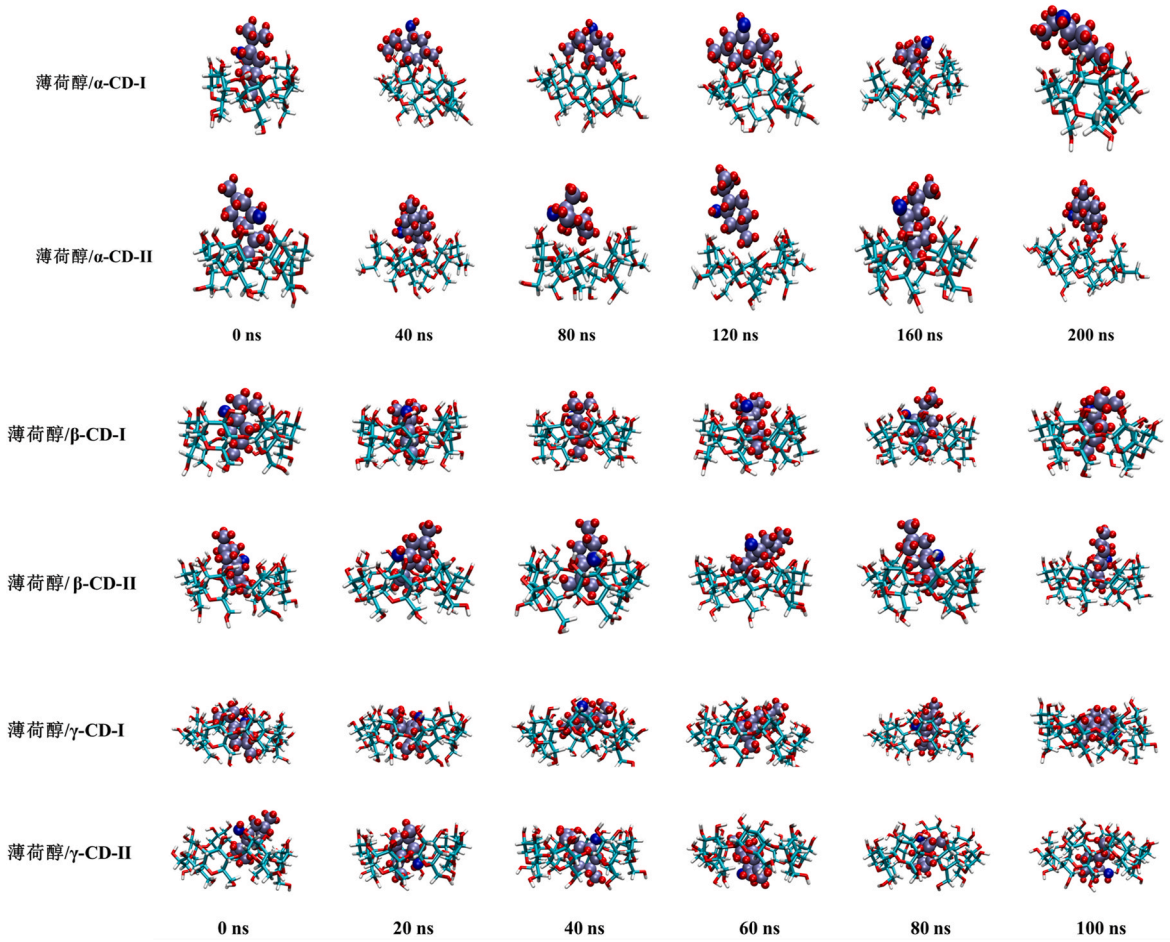

Fig. 6. Conformational changes of menthol/CD-ICs.

methyl group were exposed outside. The isopropyl group of menthol positioned at the large opening end of β-CD in menthol/β-CD-I. Compared with menthol/β-CD-I, menthol/β-CD-II has more menthol exposed outside the cavity of β-CD. This may be because the isopropyl group of menthol is located at the larger opening of β-CD, while in menthol/β-CD-II, the methyl group of menthol is at the larger opening of β-CD. The steric hindrance of the isopropyl group is greater than that of the methyl group (Deng et al., 2022). Additionally, the hydrophilicity of the large opening of β-CD is stronger, making it easier to interact with the hydroxyl group of menthol, which results in greater stability of the isopropyl group at the large opening of β-cyclodextrin. Therefore, it is speculated that the stability of menthol/β-CD-I is superior to that of menthol/β-CD-II. In the cases of menthol/γ-CD-I and menthol/γ-CD-II, menthol was entirely encapsulated by γ-CD.

3.3.3. RMSD and Rg analysis

RMSD indicates the deviation between the structure at any given moment and the initial structure. The greater the range of atomic

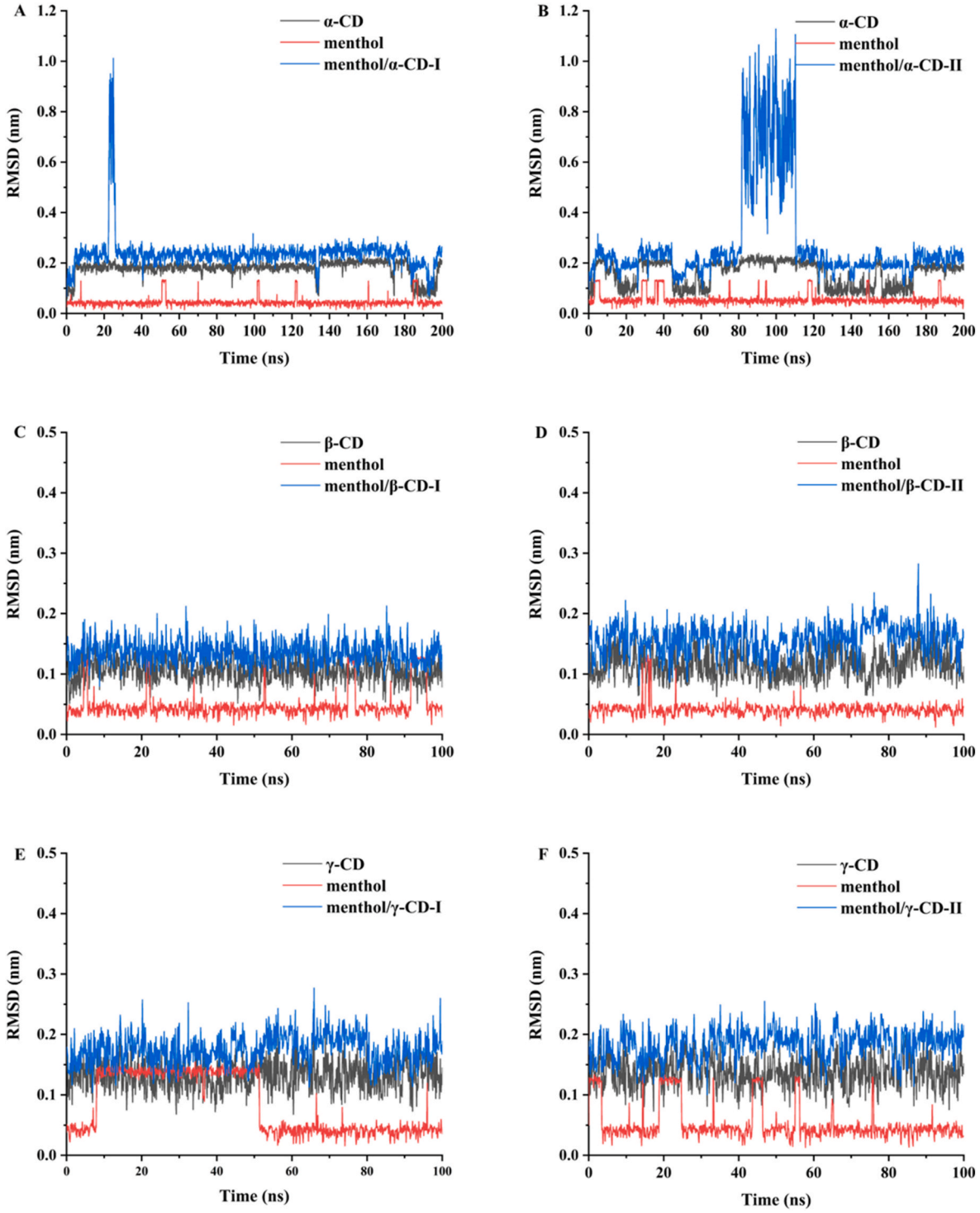

Fig. 7. Molecular structural changes. RMSD for (A) α-CD, menthol, menthol/α-CD-I; (B) α-CD, menthol, menthol/α-CD-II; (C) β-CD, menthol, menthol/β-CD-I; (D) β-CD, menthol, menthol/β-CD-II; (E) γ-CD, menthol, menthol/γ-CD-I; (F) γ-CD, menthol, menthol/γ-CD-II.

movement, the larger the RMSD value (Deng et al., 2022; Kou et al., 2023). As shown in Fig. 7A and B, the RMSD values for α-CD fluctuated significantly, alternating between 0.10 nm and 0.18 nm. This phenomenon may be attributed to the rotation of the α-1,4 glucopyranoside bonds within the α-CD. As shown in Fig. 7C–F, the average RMSD values for β-CD and γ-CD were 0.12 nm and 0.13 nm, respectively, indicating that their structural changes were more minor compared with α-CD. Compared with the free CDs, the RMSD values of the ICs increased. This may be due to the structural changes in menthol (Deng et al., 2022). The RMSD value of menthol/α-CD-I sharply increased from 0.23 nm to 1.0 nm between 22 and 25 ns and then decreased and stabilized at 0.23 nm, while the RMSD value of menthol/α-CD-II increased from 0.21 nm to 1.1 nm between 81 and 110 ns and kept at 0.21 nm. The significant fluctuations in the RMSD values demonstrated substantial departures from the initial structure (Pérez-Figueroa et al., 2024). The RMSD values of menthol/β-CD-IC and menthol/γ-CD-IC were more stable compared with menthol/α-CD-IC, which also supports the experimental result that menthol/α-CD-IC cannot be formed.

Rg is the mass-weighted average radius of a molecule. A smaller Rg indicates a more compact structure. As shown in Fig. 8A and B, the Rg values of the ICs were smaller than those of the free β-CD and γ-CD, suggesting that the menthol/β-CD-ICs and menthol/γ-CD-ICs had a more compact structure. In contrast, the Rg values of the menthol/α-CD-IC were greater than that of α-CD, implying the instability of the menthol/α-CD-IC.

3.3.4. RDF and SASA analysis

The variation in water density around the ICs was obtained through RDF (Cheng et al., 2018), as shown in Fig. 9A. The RDF plots of α-CD, β-CD, and γ-CD exhibit two peaks at r = 0.025–0.24 nm and r = 0.87–1.02 nm, corresponding to the density distribution of water inside and outside the CDs cavities (Pereva et al., 2019; Sandilya et al., 2020; Zhou et al., 2015), the distance between the two peaks for β-CD and γ-CD is essentially consistent with the cavity thickness of β-CD and γ-CD (Kou et al., 2023), however, the distance between the two peaks for α-CD is greater than the cavity thickness of α-CD, which may be attributed to the distortion of the glucose units in α-CD accompanied by significant dynamic flexibility (Sandilya et al., 2020). The order of RDF values for the CDs at 0.025–0.24 nm is: γ-CD>β-CD>α-CD, which might be attributed to the successively decreasing cavity volumes of the CDs, indicating increasing density of surrounding water molecules. In the RDF diagram of the ICs, the peak at 0.025–0.24 nm disappeared because menthol replaced water molecules in the cavity. At 0.87–1.02 nm, the peak values of RDF for CDs and the ICs are in the range of 0.9–1.25, and the RDF peaks for free CDs are higher than that of the ICs. Notably, the peak value for the menthol/α-CD-IC at 0.87–1.02 nm is much lower than that of the free α-CD, likely because most part of the menthol molecule is located outside the α-CD cavity. The above results on RDF supported previous experimental results.

Fig. 9B–D displays the RDF values of different hydroxyl oxygen atoms. The RDF peak values at r = 0.28 nm for O2, O3, and O6 are 0.93–1.09, 0.81–1.06, and 1.25–1.50, respectively. The peak value for O6 is significantly larger than those of O2 and O3, suggesting that the OH group at C6 is more prone to form hydrogen bonds with water molecules compared with those at C2 and C3, which are more likely to engage in intermolecular hydrogen bonding.

SASA refers to the solvent-accessible surface area of a molecule. The average SASA value for α-CD was 9.54 nm^2 (Fig. 10A). The SASA values for menthol/α-CD-I and menthol/α-CD-II are higher than that of α-CD. This increase may be attributed to the smaller cavity of α-CD, which leads to menthol being more inclined to stay outside the cavity, thereby increasing the surface area that interacts with the solvent, this is consistent with the results obtained from Rg. For β-CD and γ-CD, the average SASA values are 12.02 nm^2 and 13.80 nm^2, respectively. The SASA values for their corresponding ICs are reduced. This reduction is attributed to the contraction of the structure and the lower interaction with the surrounding solvent.

3.3.5. Hydrogen bonding analysis

CDs have a polyhydroxy structure that can form hydrogen bonds with menthol and water molecules. Fig. 11A illustrates the number of hydrogen bonds formed by different hydroxyl oxygen atoms, clearly showing that the hydroxyl group at the C6 position forms more hydrogen bonds than those at the C2 and C3 positions. This may be attributed to the steric hindrance of the hydroxyl group at the C6 position is smaller and its stronger polarity. From the results of hydrogen bonds shown in Fig. 11A, it was found that the number of hydrogen bonds formed between the hydroxyl group at the C2 position of the ICs and water molecules is lower compared with the number of hydrogen bonds formed between free CDs and water molecules. However, the number of hydrogen bonds formed between CDs at the C3 and C6 positions and water molecules is not significantly different from that of the ICs with water molecules. This may be due to the conformational changes of the hydroxyl group at the C2 position in menthol/CD-ICs during the simulation, which makes it a better hydrogen bond donor, thereby interacting with the hydroxyl group on menthol and resulting in a decrease in the number of hydrogen bonds formed between the hydroxyl group at the C2 position and water molecules (Sandilya et al., 2020).

Fig. 11B presents the intramolecular and intermolecular hydrogen bonds between the menthol and CDs. The number of intramolecular hydrogen bonds in menthol/CD-ICs is greater than that in free CDs, indicating that the molecular structure of CD is more stable after encapsulation. Meanwhile, the number of intermolecular hydrogen

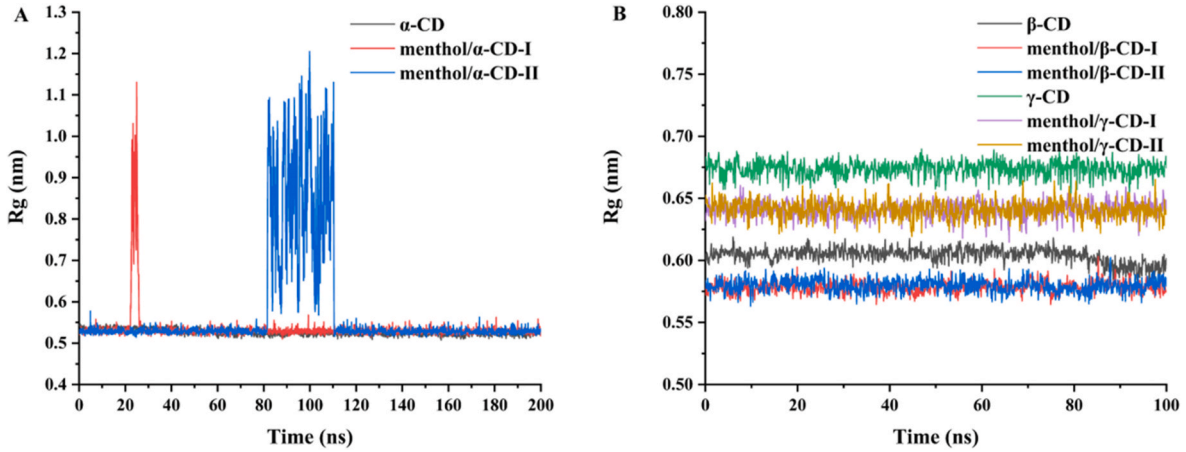

Fig. 8. Rg for (A) α-CD, menthol/α-CD-I, menthol/α-CD-II; (B) β-CD, menthol/β-CD-I, menthol/β-CD-II, γ-CD, menthol/γ-CD-I, menthol/γ-CD-II.

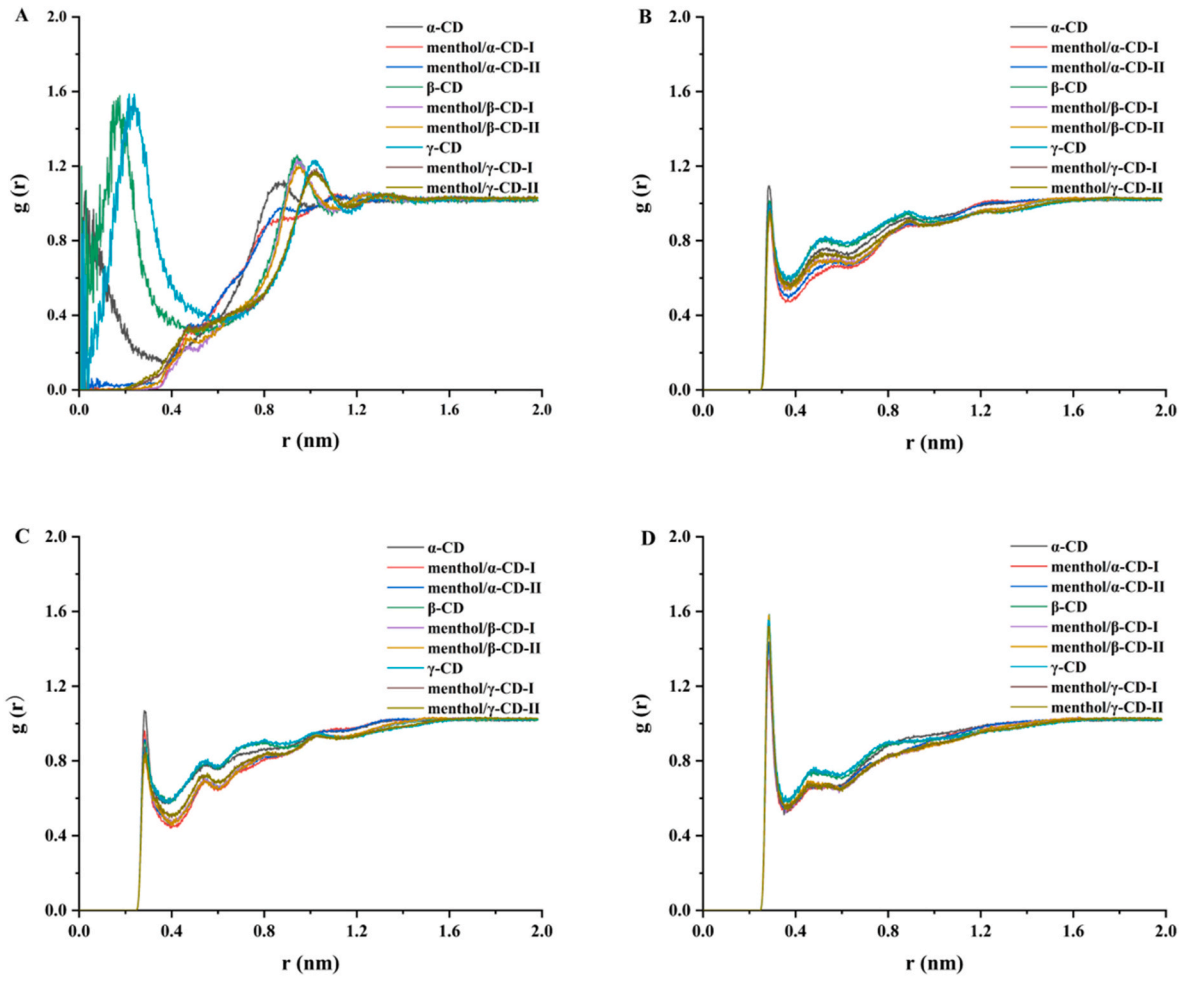

Fig. 9. Rdf for (A) CDs and ICs; (B) O2; (C) O3; (D) O6.

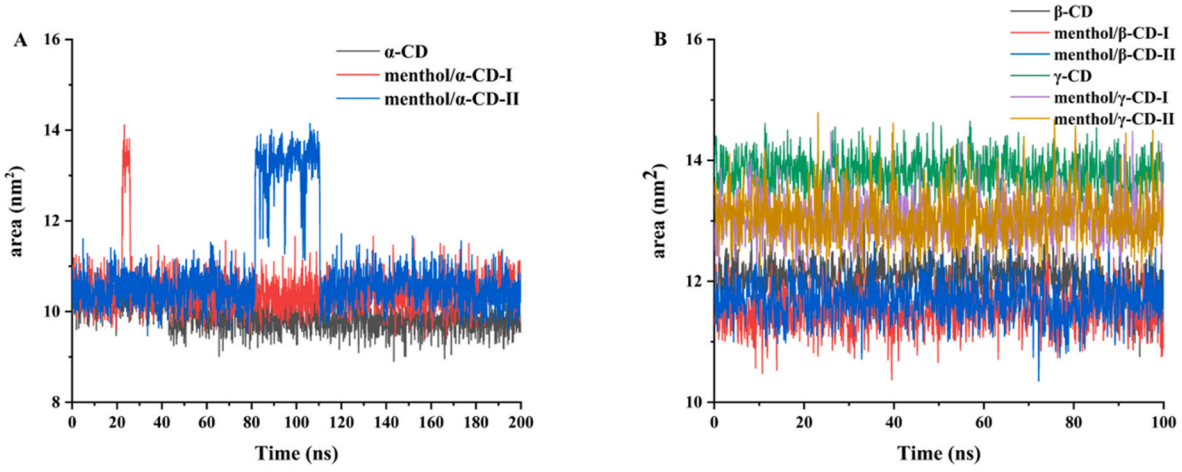

Fig. 10. SASA for (A) α-CD, menthol/α-CD-I, menthol/α-CD-II; (B) β-CD, menthol/β-CD-I, menthol/β-CD-II, γ-CD, menthol/γ-CD-I, menthol/γ-CD-II.

bonds is very few, with a slight increase after the formation of the ICs, suggesting that the hydrogen bonds formed between menthol and the three types of CDs are weak (Deng et al., 2022; Kou et al., 2023).

3.3.6. *Thermodynamic energy analysis*

As shown in Fig. 12, the van der Waals interaction energy (△Evdw) for each IC is significantly greater than the electrostatic interaction energy (△Eele), indicating that van der Waals interaction was the predominant factor between menthol and CDs (Oo et al., 2022; Sangpheak et al., 2014). Moreover, the solvation energy of the ICs is positive, which indicates that the ICs are not easily soluble in water. According to Table 3, the △Gbind of the menthol with CDs follows the order: menthol/β-CD-I > menthol/β-CD-II > menthol/γ-CD-II > menthol/γ-CD-I > menthol/α-CD-I > menthol/α-CD-II. According to the references, although menthol completely enters the cavity of γ-CD in conformational analysis, the encapsulation of guest molecules by CDs requires a

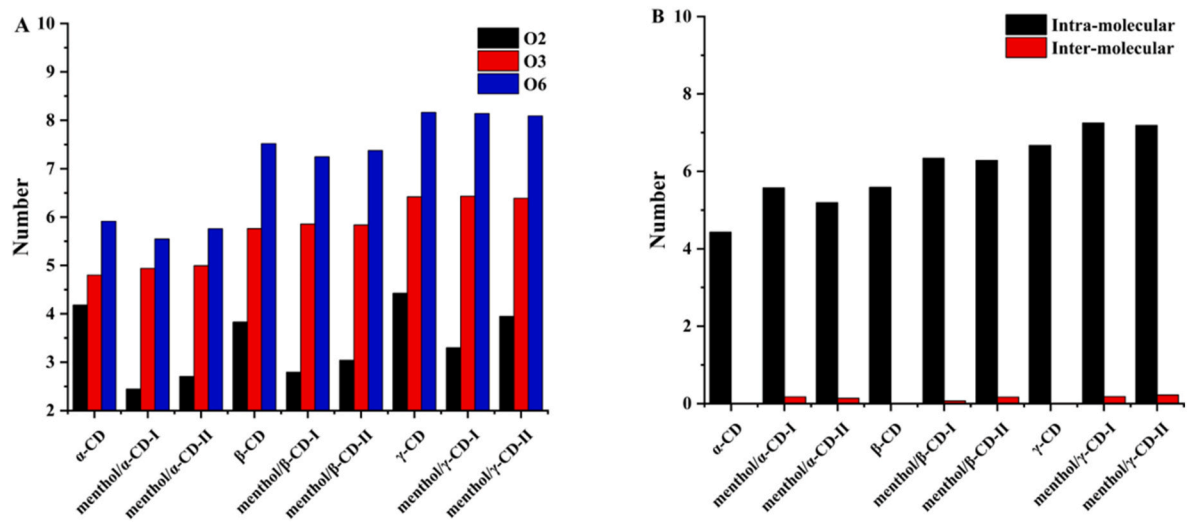

Fig. 11. (A) Hydrogen bonds formed by O atoms of different hydroxyl groups, O2, O3, and O6, were O atoms of –OH at positions C2, C3, and C6, respectively; (B) intramolecular and intermolecular hydrogen bonds.

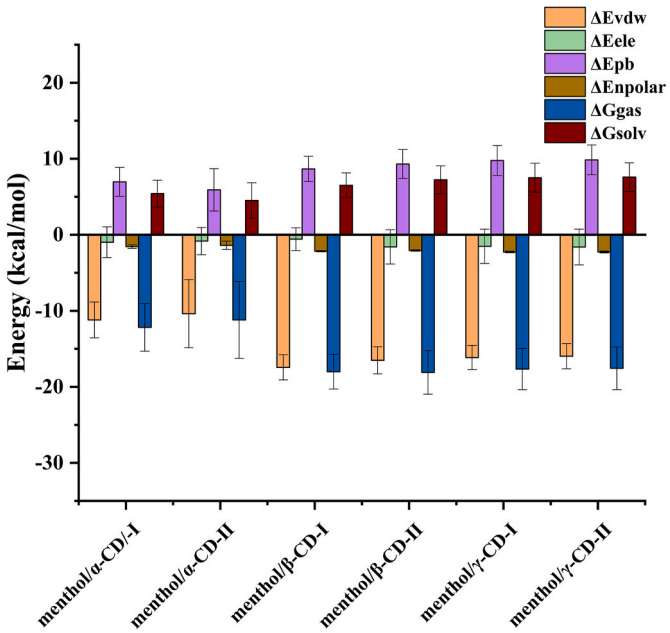

Fig. 12. Contributions of different types of energy (kcal/mol). Here, △Evdw signifies van der Waals energy; △Eele refers to electrostatic energy; △Epb represents polar solvation energy; and △Enpolar indicates nonpolar solvation energy; △ Ggas represents the average interaction energy in the gas phase; △Gsolv indicates solvation-free energy.

Table 3
Binding enthalpy (△H), interaction entropy (-T△S), and binding energy (△Gbind) of compounds.

	△H (kcal/mol)	-T△S (kcal/mol)	△Gbind (kcal/mol)
menthol/α-CD-I	−6.75 ± 2.22	9.34 ± 0.12	2.59 ± 2.22
menthol/α-CD-II	−6.69 ± 3.33	10.79 ± 0.12	4.1 ± 3.33
menthol/β-CD-I	−11.5 ± 1.55	4.23 ± 0.06	−7.27 ± 1.55
menthol/β-CD-II	−10.87 ± 1.76	4.91 ± 0.27	−5.96 ± 1.78
menthol/γ-CD-I	−10.15 ± 1.94	5.02 ± 0.32	−5.13 ± 1.96
menthol/γ-CD-II	−9.97 ± 1.97	4.78 ± 0.04	−5.19 ± 1.97

match between the size of the CDs' cavity and that of the guest molecules to achieve optimal encapsulation (Albers and Muller, 1991; Kogame-Asahara et al., 2020; Shi et al., 2023). The cavity volume of γ-CD is 462 A^3 (Kfoury et al., 2016), which is much larger than the molecular volume of menthol (291.5 A^3). Therefore, the binding free energy (△Gbind) of menthol/γ-CD-IC is greater compared with that of menthol/β-CD-IC. It can be seen from Table 3 that the binding free energy of menthol/α-CD-IC is positive, indicating that the menthol/α-CD-IC is unstable, likely due to the smaller cavity of α-CD, which cannot effectively accommodate the menthol molecule. Overall, the stability of menthol/β-CD-IC is greater than that of menthol/α-CD-IC and menthol/γ-CD-IC, and this result is consistent with the experimental results that menthol/β-CD-IC exhibits the highest EE and LE values.

4. Conclusions

This study explored the encapsulation ability of natural cyclodextrins for menthol through experimental and molecular simulation methods. The menthol/β-CD-IC and menthol/γ-CD-IC were prepared and characterized by FTIR, XRD, and TGA techniques, while the preparation of menthol/α-CD-IC was not successful. By measuring the EE and LE values, it was found that β-CD exhibited the best encapsulation ability for menthol. The comparative analysis on conformational changes, RMSD, Rg, RDF, SASA, and hydrogen bonds between CDs, menthol, and the ICs carried out through MD simulations showed that menthol/α-CD-IC is unstable, which supports the experimental result. In the subsequent binding free energy analysis. The binding free energy of menthol/β-CD-IC is the lowest, followed by menthol/γ-CD-IC, while menthol/α-CD-IC exhibits a positive binding free energy. Overall, molecular simulation results are consistent with the practical experimental results, so molecular simulation can serve as an effective screening method, an alternative to experiments, to obtain the combination ability between host-guest molecules. Subsequent studies can focus on the release kinetics of menthol/β-CD-IC and the MD simulation method can be utilized to investigate the encapsulation effects of more host-guest molecules, and for screening of wall materials.

CRediT authorship contribution statement

Sa Xu: Conceptualization, Software, Writing – original draft, Writing – review & editing. **Fang Wei:** Methodology, Investigation. **Ximing Xu:** Software. **Rui Wang:** Investigation. **Xiujuan Xu:** Investigation. **Wu Fan:** Methodology. **Guobi Chai:** Methodology. **Qidong Zhang:**

Validation. **Qingzhao Shi:** Conceptualization, Writing – original draft, Writing – review & editing.

Funding

The research was financially supported by the National Natural Science Foundation of China (Grant No. 32130083), the scientific research program of innovation platform in State Tobacco Monopoly Administration (442021AW0430), and the Young Talent Promotion Fund project of Zhengzhou Tobacco Research Institute of China National Tobacco Corporation (442020CR0330).

Declaration of competing interest

The authors declare that they have no known competing financial interests or personal relationships that could have appeared to influence the work reported in this paper.

Data availability

Data will be made available on request.

References

Albers, E., Muller, B.W., 1991. Complexation of steroid hormones with cyclodextrins derivatives: substituent effects of the guest molecule on solubility and stability in aqueous solution. J. Pharmaceut. Sci. 81 (8), 756–761. https://doi.org/10.1002/jps.2600810808.

Alvira, E., 2018. Theoretical study of the β-cyclodextrin inclusion complex formation of eugenol in water. Molecules 23 (4). https://doi.org/10.3390/molecules23040928.

Bhardwaj, V.K., Purohit, R., 2023. A comparative study on inclusion complex formation between formononetin and β-cyclodextrin derivatives through multiscale classical and umbrella sampling simulations. Carbohydr. Polym. 310. https://doi.org/10.1016/j.carbpol.2023.120729.

Cao, C., Deng, C., Hu, J., Zhou, Y., 2022. Formation and molecular dynamics simulation of inclusion complex of large-ring cyclodextrin and 4-terpineol. J. Food Sci. 87 (10), 4609–4621. https://doi.org/10.1111/1750-3841.16303.

Chang, C., Song, M., Ma, M., Song, J., Cao, F., Qin, Q., 2023. Preparation, characterization and molecular dynamics simulation of rutin–cyclodextrin inclusion complexes. Molecules 28 (3). https://doi.org/10.3390/molecules28030955.

Cheng, L., Feng, T., Zhang, B., Zhu, X., Hamaker, B., Zhang, H., Campanella, O., 2018. A molecular dynamics simulation study on the conformational stability of amylose-linoleic acid complex in water. Carbohydr. Polym. 196, 56–65. https://doi.org/10.1016/j.carbpol.2018.04.102.

Crini, G., 2014. Review: a history of cyclodextrins. Chem. Rev. 114 (21), 10940–10975. https://doi.org/10.1021/cr500081p.

Deng, C., Cao, C., Zhang, Y., Hu, J., Gong, Y., Zheng, M., Zhou, Y., 2022. Formation and stabilization mechanism of β-cyclodextrin inclusion complex with C10 aroma molecules. Food Hydrocoll. 123. https://doi.org/10.1016/j.foodhyd.2021.107013.

Duan, L., Liu, X., Zhang, J.Z.H., 2016. Interaction entropy: a new paradigm for highly efficient and reliable computation of protein–ligand binding free energy. J. Am. Chem. Soc. 138 (17), 5722–5728. https://doi.org/10.1021/jacs.6b02682.

Eberhardt, J., Santos-Martins, D., Tillack, A.F., Forli, S., 2021. AutoDock Vina 1.2.0: new docking methods, expanded force field, and Python bindings. J. Chem. Inf. Model. 61 (8), 3891–3898. https://doi.org/10.1021/acs.jcim.1c00203.

Han, P., Zhong, Y., An, N., Lu, S., Wang, Q., Dong, J., 2021. Preparation, characterization, and molecular modeling of sesamol/β-cyclodextrin derivatives inclusion complexes. J. Mol. Liq. 339. https://doi.org/10.1016/j.molliq.2021.116790.

He, N., Zhang, C., Hou, K., Yu, H., Zhang, D., Chen, M., Zhang, K., Wang, X., 2023. A comprehensive study on flavor/cyclodextrin inclusion complexes. Colloids Surf. A Physicochem. Eng. Asp. 679. https://doi.org/10.1016/j.colsurfa.2023.132613.

Hu, X., Zeng, Z., Zhang, J., Wu, D., Li, H., Geng, F., 2023. Molecular dynamics simulation of the interaction of food proteins with small molecules. Food Chem. 405. https://doi.org/10.1016/j.foodchem.2022.134824.

Hu, Z., Li, S., Wang, S., Zhang, B., Huang, Q., 2021. Encapsulation of menthol into cyclodextrin metal-organic frameworks: preparation, structure characterization and evaluation of complexing capacity. Food Chem. 338. https://doi.org/10.1016/j.foodchem.2020.127839.

J, S., 1998. introduction-and-general-overview-of-cyclodextrin-chemistry. Chem. Rev. (Washington, DC, U. S.). https://doi.org/10.1021/cr970022c.

Kfoury, M., Hădărugă, N.G., Hădărugă, D.I., Fourmentin, S., 2016. Cyclodextrins as encapsulation material for flavors and aroma. In: Encapsulations, pp. 127–192. https://doi.org/10.1016/b978-0-12-804307-3.00004-1.

Kim, S., Chen, J., Cheng, T., Gindulyte, A., He, J., He, S., Li, Q., Shoemaker, B.A., Thiessen, P.A., Yu, B., Zaslavsky, L., Zhang, J., Bolton, E.E., 2018. PubChem 2019 update: improved access to chemical data. Nucleic Acids Res. 47 (D1), D1102–D1109. https://doi.org/10.1093/nar/gky1033.

Kogame-Asahara, C., Ito, S., Iguchi, H., Kazama, A., Shigemitsu, H., Kida, T., 2020. A novel molecular tube fully modified at one end: selective inclusion of cis-unsaturated fatty acid esters. Chem. Commun. 56 (9), 1353–1356. https://doi.org/10.1039/c9cc08709e.

Kou, X., Zhang, Y., Su, D., Wang, H., Huang, X., Niu, Y., Ke, Q., Xiao, Z., Meng, Q., 2023. Study on host-guest interaction of aroma compounds/γ-cyclodextrin inclusion complexes. Lwt 178. https://doi.org/10.1016/j.lwt.2023.114589.

Kumar, P., Bhardwaj, V.K., Purohit, R., 2023. Dispersion-corrected DFT calculations and umbrella sampling simulations to investigate stability of Chrysin-cyclodextrin inclusion complexes. Carbohydr. Polym. 319. https://doi.org/10.1016/j.carbpol.2023.121162.

Kumar, P., Bhardwaj, V.K., Purohit, R., 2024. Highly robust quantum mechanics and umbrella sampling studies on inclusion complexes of curcumin and β-cyclodextrin. Carbohydr. Polym. 323. https://doi.org/10.1016/j.carbpol.2023.121432.

Kumar, P., Purohit, R., 2024. Driving forces and large scale affinity calculations for piperine/γ-cyclodxetrin complexes: mechanistic insights from umbrella sampling simulation and DFT calculations. Carbohydr. Polym. 342. https://doi.org/10.1016/j.carbpol.2024.122350.

Lin, Y., Huang, R., Sun, X., Yu, X., Xiao, Y., Wang, L., Hu, W., Zhong, T., 2022. The p-Anisaldehyde/β-cyclodextrin inclusion complexes as a sustained release agent: characterization, storage stability, antibacterial and antioxidant activity. Food Control 132. https://doi.org/10.1016/j.foodcont.2021.108561.

Mazurek, A.H., Szeleszczuk, Ł., Gubica, T., 2021. Application of molecular dynamics simulations in the analysis of cyclodextrin complexes. Int. J. Mol. Sci. 22 (17). https://doi.org/10.3390/ijms22179422.

Oo, A., Kerdpol, K., Mahalapbutr, P., Rungrotmongkol, T., 2022. Molecular encapsulation of emodin with various β-cyclodextrin derivatives: a computational study. J. Mol. Liq. 347. https://doi.org/10.1016/j.molliq.2021.118002.

Pereva, S., Nikolova, V., Angelova, S., Spassov, T., Dudev, T., 2019. Water inside β-cyclodextrin cavity: amount, stability and mechanism of binding. Beilstein J. Org. Chem. 15, 1592–1600. https://doi.org/10.3762/bjoc.15.163.

Pérez-Figueroa, S.E., Galván-García, E.A., Nivón-Ramírez, D., Ramos, E., Gómez-Balderas, R., 2024. Chlorpropamide-cyclodextrin inclusion complexes, theoretical basis of stability. J. Mol. Liq. 396. https://doi.org/10.1016/j.molliq.2024.123995.

Phunpee, S., Saesoo, S., Sramala, I., Jarussophon, S., Sajomsang, W., Puttipipatkhajorn, S., Soottitantawat, A., Ruktanonchai, U.R., 2016. A comparison of eugenol and menthol on encapsulation characteristics with water-soluble quaternized β-cyclodextrin grafted chitosan. Int. J. Biol. Macromol. 84, 472–480. https://doi.org/10.1016/j.ijbiomac.2015.11.006.

Sandilya, A.A., Natarajan, U., Priya, M.H., 2020. Molecular view into the cyclodextrin cavity: structure and hydration. ACS Omega 5 (40), 25655–25667. https://doi.org/10.1021/acsomega.0c02760.

Sangpheak, W., Khuntawee, W., Wolschann, P., Pongsawasdi, P., Rungrotmongkol, T., 2014. Enhanced stability of a naringenin/2,6-dimethyl β-cyclodextrin inclusion complex: molecular dynamics and free energy calculations based on MM- and QM-PBSA/GBSA. J. Mol. Graph. Model. 50, 10–15. https://doi.org/10.1016/j.jmgm.2014.03.001.

Shi, Q., Chai, G., Xu, X., Fan, W., Wu, C., Ji, L., Xi, H., Mao, J., Liu, J., Song, Y., Zhang, Q., 2023. A strategy to maintain the organoleptic quality of flavor-β-cyclodextrin inclusion complexes: characteristics aroma reconstruction of Osmanthus absolute. Lwt 176. https://doi.org/10.1016/j.lwt.2023.114570.

Trott, O., Olson, A.J., 2009. AutoDock Vina: improving the speed and accuracy of docking with a new scoring function, efficient optimization, and multithreading. J. Comput. Chem. 31 (2), 455–461. https://doi.org/10.1002/jcc.21334.

Valdés-Tresanco, M.S., Valdés-Tresanco, M.E., Valiente, P.A., Moreno, E., 2021. gmx_MMPBSA: a new tool to perform end-state free energy calculations with GROMACS. J. Chem. Theor. Comput. 17 (10), 6281–6291. https://doi.org/10.1021/acs.jctc.1c00645.

Vanommeslaeghe, K., Hatcher, E., Acharya, C., Kundu, S., Zhong, S., Shim, J., Darian, E., Guvench, O., Lopes, P., Vorobyov, I., Mackerell, A.D., 2009. CHARMM general force field: a force field for drug-like molecules compatible with the CHARMM all-atom additive biological force fields. J. Comput. Chem. 31 (4), 671–690. https://doi.org/10.1002/jcc.21367.

Wang, H., Meng, F., 2017. The permeability enhancing mechanism of menthol on skin lipids: a molecular dynamics simulation study. J. Mol. Model. 23 (10). https://doi.org/10.1007/s00894-017-3457-y.

Wu, Y., Xiao, Y., Yue, Y., Zhong, K., Zhao, Y., Gao, H., 2020. A deep insight into mechanism for inclusion of 2R,3R-dihydromyricetin with cyclodextrins and the effect of complexation on antioxidant and lipid-lowering activities. Food Hydrocoll. 103. https://doi.org/10.1016/j.foodhyd.2020.105718.

Xiao, Z., Hou, W., Kang, Y., Niu, Y., Kou, X., 2019. Encapsulation and sustained release properties of watermelon flavor and its characteristic aroma compounds from γ-cyclodextrin inclusion complexes. Food Hydrocoll. 97. https://doi.org/10.1016/j.foodhyd.2019.105202.

Yin, H., Wang, C., Yue, J., Deng, Y., Jiao, S., Zhao, Y., Zhou, J., Cao, T., 2021. Optimization and characterization of 1,8-cineole/hydroxypropyl-β-cyclodextrin inclusion complex and study of its release kinetics. Food Hydrocoll. 110. https://doi.org/10.1016/j.foodhyd.2020.106159.

Zhang, X., Su, J., Wang, X., Wang, X., Liu, R., Fu, X., Li, Y., Xue, J., Li, X., Zhang, R., Chu, X., 2022. Preparation and properties of cyclodextrin inclusion complexes of hyperoside. Molecules 27 (9). https://doi.org/10.3390/molecules27092761.

Zhou, G., Zhao, T., Wan, J., Liu, C., Liu, W., Wang, R., 2015. Predict the glass transition temperature and plasticization of β-cyclodextrin/water binary system by molecular dynamics simulation. Carbohydr. Res. 401, 89–95. https://doi.org/10.1016/j.carres.2014.10.026.